HHS Public Access

Author manuscript

Cancer Res. Author manuscript; available in PMC 2018 April 15.

Published in final edited form as:

Cancer Res. 2017 April 15; 77(8): 2124–2133. doi:10.1158/0008-5472.CAN-15-2870.

Distinct Levels of Radioresistance in Lgr5+ Colonic Epithelial Stem Cells versus Lgr5+ Small Intestinal Stem Cells

Guoqiang Hua[1,2,3], **Chu Wang**[1], **Yan Pan**[1,2], **Zhaoshi Zeng**[4], **Sang Gyu Lee**[1], **Maria Laura Martin**[2,4], **Adriana Haimovitz-Friedman**[3], **Zvi Fuks**[3,*], **Philip B. Paty**[4,*], and **Richard Kolesnick**[2,*]

[1]Institute of Radiation Medicine, Fudan University, Shanghai, China

[2]Laboratory of Signal Transduction, Memorial Sloan Kettering Cancer Center, New York, NY; USA

[3]Department of Radiation Oncology, Memorial Sloan Kettering Cancer Center, New York, NY; USA

[4]Department of Surgery, Memorial Sloan Kettering Cancer Center, New York, NY. USA

Abstract

While small and large intestines possess seemingly similar Wnt-driven Leucine-rich repeat-containing G protein coupled receptor 5 (Lgr5)+ adult epithelial stem cells, we report here that the two organs exhibit distinct mechanisms of tissue response to ionizing radiation. Employing Lgr5-lacZ transgenic mice and Lgr5 in situ hybridization, we found colonic epithelial stem cells (CESCs) markedly more radioresistant in vivo than small intestinal crypt base columnar stem cells (CBCs) ($D0 = 6.0 \pm 0.3$ Gy vs. 1.3 ± 0.1, respectively; $p<0.01$). Accordingly, CESCs survived 30 Gy exposure, while CBCs were completely depleted after 15 Gy. Edu incorporation studies indicated that after 19 Gy, CBCs exited growth arrest at 12 hours, resuming normal mitotic activity despite 60% of this population displaying residual γH2AX foci, indicative of persistent unrepaired DNA damage. Checkpoint recovery before complete DSB repair represents the sine qua non of a newly-defined potentially-lethal pathophysiology termed checkpoint adaptation. In the small intestinal mucosa, checkpoint adaptation resulted in CBCs succumbing to an eight-fold increase in incidence of highly-lethal chromosomal aberrations and mitotic catastrophe by 48 hours post-radiation. In contrast, Lgr5+ CESCs displayed delayed checkpoint recovery at 48 hours post-19 Gy, coordinated with complete DSB repair and regeneration of colonic mucosa originating, at least in part, from surviving CESCs. The discovery that small intestinal CBCs succumb to checkpoint adaptation is the first demonstration that this aberrant cell cycle response may drive mammalian tissue radiosensitivity.

Keywords

Radiation; Intestinal stem cells; Mitotic cell death; Lgr5; Colonic epithelial stem cells

Correspondence should be addressed to: Richard Kolesnick MD, Laboratory of Signal Transduction, Memorial Sloan-Kettering Cancer Center, 1275 York Avenue, New York, NY 10065; Telephone: 646-888-2096, Fax: 646-422-0281; r-kolesnick@ski.mskcc.org; guoqianghua@fudan.edu.cn.

*Equal co-authors

Disclosures: No potential conflicts of interest were disclosed

INTRODUCTION

The differential response of mammalian tissues to high doses of ionizing radiation is posited in terms of differences in radiosensitivity of tissue stem cell compartments (1–3), although no definitive study corroborating this widely-held hypothesis has ever been published. This is because until recently validated solid tissue stem cells were not available for direct study. While it is well documented that the large intestine is more radioresistant than the small intestine, mechanisms underlying large intestine radioresistance remain poorly understood (4, 5). Here we compare two highly similar Wnt-driven Lgr5+ (also known as Gpr49) (6, 7) intestinal stem cell (ISC) populations at the base of the crypts of the small and large intestine in an attempt to elucidate mechanisms controlling radiosensitivity.

Of currently studied adult stem cell populations in mammalian organs, response of the small intestinal Lgr5+ crypt base columnar cell (CBC) to genotoxic stress is perhaps the best studied. The small intestinal mucosa is a rapid turnover system, considered driven by mitotic activity of self-renewing Lgr5+ CBCs (6, 7). Prior to discovery of the Lgr5+ CBC, survival of ISCs to genotoxic stress was quantified indirectly using the Microcolony Assay (also termed Clonogenic Assay) of Withers and Elkind (8) by counting regenerating crypts in histologic sections at 3.5 days post radiation. The rationale of this assay, regarded as one of the best surrogate assays for adult mammalian stem cell responses for decades, is that it must have taken at least one stem cell to regenerate a complete crypt.

Discovery that the CBC, most often located between Paneth cells at the base of the small intestinal crypt (9) is a legitimate ISC, represents a milestone in the GI field, and has permitted detailed analysis of its response to genotoxic stress. While many groups have confirmed that the threshold for survivability of the small intestine to ionizing radiation is approximately 10% regenerative crypts at 3.5 days after irradiation as determined by the Microcolony Assay (10–12), we determined that death of CBCs preceded crypt regeneration, detectable at 1 day post irradiation and maximal at 2 days (13, 14). Furthermore, loss of CBCs predicted outcome of the Microcolony Assay as one might anticipate if CBCs represented the relevant target for small intestinal survival. Loss of CBCs within the first 2 days post irradiation was biphasic with about 30% of CBCs dying by apoptosis during the first 24 hours after 12 Gy, while cells are growth arrested and repairing DNA damage, followed by mitotic death of approximately 60% of CBCs during the subsequent 24 hours, leaving a residual of 10% of CBCs available for crypt regeneration. That CBCs were relevant ISCs for organ recovery was indicated by lineage tracing studies post-irradiation. At 15 Gy, a dose that reduces crypt counts by 95–99% in the Withers and Elkind analysis, and is not survivable, complete loss of CBCs was detected by 48 hours post irradiation. Further study revealed that of all the cell populations of the small intestinal crypt/villus unit, the Lgr5+ CBC was the most radioresistant due to efficient use of error-free homologous recombination to repair double strand breaks.

Like the small intestine, the large intestine is maintained by a rapidly cycling population of Wnt-driven Lgr5+ colonic epithelial stem cells (CESCs) that reside at the crypt base in between a cKit+ population of niche cells. In the current study, we profile these two highly

similar Lgr5+ stem cell populations in the large and small intestine. We show that Lgr5+ CESCs in the distal large intestine are far more radiation resistant than their counterparts in the small intestine, differences attributable to substantive differences in cell cycle re-entry and the propensity to undergo mitotic death. Activation of cell cycle checkpoints by DSBs that transiently arrest cell cycle progression is critical in optimizing DSB repair and maintaining genomic integrity (15). Accordingly, tight coordination between DSB repair and checkpoint recovery constitutes a generic function of a high fidelity DNA damage response (DDR) (16). Recently, however, a pathophysiologic alternative checkpoint dynamic has been described, termed checkpoint adaptation [reviewed in (16, 17)], an uncoupling of completion of DSB repair and checkpoint recovery that enables precocious cell cycle progression in the presence of residual unrepaired DNA (18). G2M transition in the presence of unrepaired DNA renders kinetochore/mitotic spindle dysfunction during segregation of damaged DNA strands (19), promoting toxic chromosomal re-arrangements, genomic instability and reproductive (also termed clonogenic) lethality (20). Hence, while the mechanism driving dysfunctional checkpoint adaptation remains to a large extent unknown (17), it predisposes affected cells to mitotic catastrophe. Here we show CBCs are subject to checkpoint adaptation, which drives a unique mechanism of small intestinal tissue radiosensitivity, while CESCs maintain a fully-controlled checkpoint recovery, coordinated with completion of DSB repair, conferring a radioresistant colonic tissue phenotype.

MATERIALS AND METHODS

Mice

Lgr5-lacZ and Lgr5-EGFP-ires-CreERT2/Rosa26-lacZ were genotyped and used as described (6, 13). All mice were maintained on a C57BL/6 background. Mouse protocols were approved by Memorial Sloan Kettering Cancer Center Institutional Animal Care and Use Committee.

Irradiation

Whole-body radiation (WBR) was delivered with a Shepherd Mark-I unit (Model 68, SN643, J. L. Shepherd & Associates, San Fernando, CA) operating ^{137}Cs sources at 1.72 Gy/min. Distal colon irradiation was delivered with 250 kVp X-ray produced by X-Rad 320 with 0.25 mm Cu filtration as per published method with minor modifications. Briefly, anesthetized mice were placed and irradiated in a close-fitting jig. The jig was covered by a 5 mm-thick lead shield except for a 2.0 × 1.0 cm rectangular aperture enabling precise targeting of the distal colon. Field uniformity and dose homogeneity were defined using a 16 mm thick Superflab phantom, with an IBA CC04 ionization chamber placed at 8 mm, and by exposing Kodak XV film for density contour using a densitometer. Crypt and ISC survival curves were calculated by least square regression analysis, with a modification of the FIT software program, as previously published (21). The program fits curves by iteratively weighted least squares to each set of dose-survival data, estimates covariates of survival curve parameters and corresponding confidence regions, and plots the survival curve. It also derives curve parameters, such as the D_0, the reciprocal of the slope on the exponential portion of the curve, representing the level of radiosensitivity.

Tissue preparation

Intestinal tissue samples were fixed by 16–18 h incubation in 4% freshly prepared neutral buffered formaldehyde (21), and embedded in paraffin blocks. Transverse sections of the full intestinal circumference were prepared and stained with hematoxylin and eosin as described (13).

β-galactosidase (lacZ) staining

Lgr5-lacZ mice were euthanized after radiation, and four 2.5 cm-sequential segments of proximal jejunum from the ligament of Treitz, or 2-cm segment of distal colon were obtained. Staining for presence of β-galactosidase was as per (6).

Crypt Microcolony Assay

The Microcolony Assay was performed as described by Withers and Elkind (8). Briefly, at 3.5 days (small intestine) or 5 days (distal colon) after irradiation intestines were obtained and hematoxylin and eosin stained as above. Surviving crypts were defined as containing 10 or more adjacent chromophilic cells and a lumen. The circumference of a transverse cross-section of the intestines was used as a unit. Number of surviving crypts was counted per circumference.

EdU incorporation assay

Lgr5-lacZ mice, 6–8 weeks old, were injected intraperitoneally with 100 μl of 20 mM EdU solution 2 hours before sacrifice (22). Distal colons were collected for paraffin embedding and EdU staining. EdU was detected with the Click-iT® EdU cell proliferation kit according to manufacturer's instruction (Invitrogen).

Caspase 3 and Lgr5 in-situ hybridization (ISH) double staining on consecutive sections

Consecutive 5 μm thick sections were used for double staining of caspase 3 and Lgr5 in situ. Apoptotic crypt cells were identified by caspase 3 staining of the active fragment. 5 μm sections were deparaffinized and rehydrated through graded ethanol. Endogenous peroxidase activity was blocked for 5 min with PBS containing 0.3% H_20_2. Antigen retrieval was performed by boiling sections for 15 min in 0.1 M citrate buffer (pH 6.0). Non-specific antibody binding was blocked for 30 min by incubation with 10% normal goat serum. Sections were incubated with rabbit anti-caspase-3 (Cell Signaling, #9661; 1:100 dilution) overnight at 4°C in a humidified chamber. Primary antibody was visualized using biotinylated goat-anti-rabbit secondary antibody and developed with an ABC kit and DAB. ISH employed the QuantiGene ViewRNA ISH Tissue 2-plex Assay kit (QVT0012) according to manufacturer’s instructions using Lgr5 (mouse VB1-10818) and GAPDH (mouse VB1-10150) probes from Affymetrix. GAPDH ISH confirmed mRNA integrity of all samples.

Lineage tracing in the large intestine

Lgr5-EGFP-ires-CreERT2/Rosa26-lacZ mice were injected intraperitoneally with a single dose of tamoxifen (4 mg/25 g mouse) immediately after 19 Gy distal colon irradiation. Mice

were sacrificed at day 0, 7 and 12 post irradiation, and distal colons were collected and stained for lacZ as per (6, 13).

Immunofluorescence staining

Paraffin-embedded tissue sections were de-waxed, rehydrated and stained with antibodies, using standard procedures (13). Primary antibodies for immunofluorescence were mouse monoclonal anti-H2AX Ser139 (JBW301, Upstate Biotechnology; dilution 1:2000), polyclonal goat anti-lysozyme (Santa Cruz, sc-27958; dilution 1:500), polyclonal goat anti-cKit (R&D, AF-1356; dilution 1:400). Multi-channel fluorescence images were acquired using an upright widefield Zeiss Axio2 Imaging microscope with AxioCam MRm Camera.

Scoring chromosomal aberrations in crypt epithelial cells

Intestinal tissues, harvested and processed as above, were stained with hematoxylin and eosin as per (13), and mitoses were scored by visual inspection at 400× magnification. Normal mitoses were scored when a cell was undergoing mitosis and condensed chromosomes aligned symmetrically. Aberrant mitoses were scored when condensed chromosomes showed multipolar spindles, lagging or misaligned chromosomes, anaphase bridges, or micronuclei as per (23, 24).

Statistical analysis

Values represent mean±SD or SEM. Differences were analyzed by Student's t test. A P value ≤0.05 was considered significant.

RESULTS

Lgr5+ CESCs are far more radioresistant than their small intestinal counterparts

Initial studies examined the dose response of intestinal crypts and Lgr5+ ISCs to whole body radiation (WBR). The crypt regeneration process was studied using the Microcolony Assay, standardized to measure number of regenerating crypts per intestinal circumference at day 3.5 post-radiation for small intestine and at day 5 for large intestine (4), as a surrogate for stem cell survival. In the small intestine of *Lgr5-lacZ* transgenic reporter mice (Figure 1A), 15 Gy WBR, which results in this strain in 100% lethality from the Radiation GI Syndrome (13), yields total depletion of Lgr5+ ISCs (blue cells at the crypt base) and complete loss of crypts. In contrast, distal colon crypts are significantly more radioresistant displaying a combination of degenerating crypts (thin walled, white arrows) and regenerating crypts (violaceous thick walled, black arrows) after 15 Gy and 19 Gy (Figure 1B). Consistent with Lgr5+ ISCs as representing critical determinants of the radioresistance of the colon, Lgr5+ ISCs remain detectable at 15 Gy and 19 Gy (Figure 1C). Radiation dose survival analysis of the small intestinal and colonic crypts and ISCs, performed over a wide range of doses (8–30 Gy) (Figure 1D), confirmed large intestinal crypts are markedly radioresistant with a D_0=2.1±0.1 Gy compared to small intestinal crypts that manifest a D_0=0.9±0.1 ($p<0.01$). Even greater disparity was observed when comparing large and small Lgr5+ ISCs that display D_0= 6.0±0.3 Gy and D_0=1.3±0.1 values, respectively ($p<0.01$), a very large 4.6-fold difference.

Radioresistant Lgr5+ CESCs repopulate colonic crypts

To investigate impact of Lgr5+ ISCs on regeneration of the colon after high dose ionizing radiation in the absence of concomitant damage to the small intestine, we engineered a specialized colorectal jig modified from published literature (25, 26). The jig was designed to frame the distal colon, based on anatomical and computerized tomography (27) data, localizing a large intestinal area restricted to the pelvis. Radiation was delivered through a 2.0×1.0 cm aperture, thus specifically targeting the distal colon while avoiding other regions of the intestinal tract (Figure 2A). Whereas orthovoltage radiation, as used here, also causes epilation restricted to the exposed skin, Figure 2B shows the rectangle of fur loss at 40 days, serving as a biological marker of the incident beam. Figure 2C presents the total large intestinal section in the standardized Swiss Roll configuration (28) and reveals radiation damage to intestinal mucosa at day 5 post irradiation was confined to distal colonic tissue (Figure 2C).

Using this strategy, *Lgr5-lacZ* mice were treated with 19 Gy WBR, a dose normally lethal to mice from the small intestinal Radiation GI Syndrome at 5 days. Figure 2D reveals that 5 days is the nadir for both crypts and CESCs in the distal colon after 19 Gy, with recovery after 7 days. Unlike the small intestine in which loss of CBCs and crypts occur in parallel (13), in the large intestine <2% of crypts survive at day 5 after 19 Gy (Figure 2E, upper panel), yet >40% of CESCs survive within the injured mucosa (Figure 2E, lower panel). The most parsimonious interpretation of these data is that Lgr5+ CESCs constitute the most radioresistant population within colonic crypts, which then serve as a stem cell pool to regenerate crypts post radiation, preserving large intestinal mucosa integrity. Furthermore, many crypts display clustering of LacZ-positive CESCs at the colonic crypt base at day 10 after 19 Gy (Figure 2D), consistent with the extensive crypt fission often observed at this time post-irradiation.

To establish whether surviving Lgr5+ CESCs result in colonic tissue regeneration after irradiation, we performed lineage-tracing assays using Lgr5-EGFP-ires-CreERT2/Rosa26-lacZ mice. Figure 3 shows Lgr5+ CESC-derived lacZ lineage tracing crypt units after 19 Gy, indicating that Lgr5+ CESCs represent a population, at least in some crypts, that regenerates epithelium post irradiation.

Lgr5+ CESCs are resistant to mitotic cell death rather than apoptosis

While our prior studies revealed small intestinal Lgr5+ CBCs show biphasic apoptotic/mitotic lethality post radiation, it should be noted that mammalian cells not undergoing apoptosis normally experience growth arrest of about 1 hour per Gy delivered, a number confirmed in our prior study in the small intestines (13). During growth arrest, mammalian cells attempt to repair potentially-lethal DNA double strand breaks, constituting a generic response of eukaryotic cells to ionizing radiation (15). Initial screening studies quantifying extent of Lgr5+ ISC loss in the small and large intestine during the first and second 24 hour time periods post 19 Gy (Figure 4A,B) revealed a similar loss of about 1/3 of small and large ISCs during the first 24-hour time period, while there was disparate loss during the second 24-hour period. Whereas the remaining 2/3 of CBCs in the small intestine were deleted during the second 24-hour period, no significant loss occurred in the large intestine. Because

these studies depended on use of in-situ hybridization (Lgr5 mRNA), we repeated these studies identifying Lgr5+ ISCs using *LacZ* reporter gene and obtained virtually identical results (Figure 4C).

To understand mechanism of ISC death, we first compared induction of apoptosis in the small and large Lgr5+ ISC populations. Figure 4D shows that in the current study 19 Gy causes an immediate apoptotic response in the ISCs of the small intestine detected by caspase3 staining, consistent with our published data (13). The pattern and extent of caspase3-positive Lgr5+ CESCs in distal colon was similar, peaking at 6 hours post radiation, and not statistically different from the small intestine (0.79±0.08 apoptotic CBCs/crypt vs. 0.64±0.08 apoptotic CESCs/crypt; $p>0.05$). Thus, differences in apoptotic cell death are likely not the reason for differences in radiosensitivity profiles.

CESCs repair DNA damage more efficiently than CBCs

Mammalian cells undergo mitotic arrest post-irradiation to facilitate DNA repair, which can be evaluated indirectly by examining kinetics of resolution of γ-H2AX ionizing radiation-induced repair foci (IRIF), a quantitative surrogate of the repair process. Figure 5A shows that CBCs and CESCs resolve IRIF at different rates with CBCs resolving IRIF more slowly, resulting in statistical differences in number of cells displaying detectable γ-H2AX foci by 12 hours post-irradiation (Figure 5B; $p<0.01$), a difference that persists until at least 18 hours, a time at which CESCs have fully resolved IRIF.

Small intestine CBCs re-enter the cell cycle before completing DNA repair

To evaluate potential differences in the period of growth arrest post irradiation, we employed EdU staining to identify (Figure 6A) and quantify (Figure 6B) cells undergoing mitosis. While both small and large intestinal crypts show numerous dividing ISCs and progenitors preceding 19 Gy irradiation, at 12 hours post irradiation cycling cells are not detected in either small or large intestinal crypts. However, CBCs begin cycling after 12 hours and by 15 hours maximal division is re-instituted (1.7±0.1 Edu+ CBCs/crypt). By comparing γH2AX data in Figure 5 with Edu data in Figure 6 it is estimated that ~60% of 19 Gy-irradiated CBCs have not completed DNA repair at the time cell division re-initiates indicating CBCs are subject to checkpoint adaptation. Consistent with this notion, we find that over the ensuing 24 hours, all of the mitotically-active small intestinal CBCs die precipitously. In contrast, CESCs begin to exit growth arrest at 24 hours post-irradiation (0.5±0.1 Edu+ CESCs/crypts) and reach pre-radiation cycling levels by 48 hours post 19 Gy. Whereas, the γH2AX data in Figure 5 indicate DSB repair is complete by 18 hours, a time preceding checkpoint recovery initiation, these data indicate that large bowel CESCs do not undergo checkpoint adaptation.

Lgr5+ CESCs display less aberrant mitoses than small intestine ISCs post irradiation

Whereas checkpoint adaptation predisposes affected cells to genomic instability and mitotic death (17), we quantified chromosomal aberrations in the crypts of the small and large intestine post irradiation (29). In unirradiated mice, all crypt cells undergoing mitosis display symmetrically-aligned chromosomes (Figure 7A). At 24 hours after 19 Gy WBR, mitotic cells in both small and large intestine display aberrant mitoses. Common abnormal

mitoses include anaphase bridges, multipolar spindles, misaligned chromosomes and chromosomal lagging (23, 24). Consistent with our γH2AX/Edu data indicating CBCs but not CESCs are subject to checkpoint adaptation, we find significantly more aberrant mitotic figures in small intestinal crypts compared with large intestinal crypts, 0.41±0.04 vs. 0.05±0.01 aberrant mitoses/crypt, respectively, an 8-fold difference (Figure 7B, $p<0.01$).

DISCUSSION

This study provides a unique comparison of two highly similar Lgr5+ adult stem cell populations. While it would have been reasonable to anticipate that the large intestinal Lgr5+ ISC would be more radioresistant than the small intestinal Lgr5+ CBC, much of what has been learned in the course of the present studies could not have been anticipated. Indeed, we find D_0 values of dose survival curves confirm colonic CESCs to be significantly more radioresistant than small intestinal CBCs, which according to classical tenets of mammalian radiobiology would be interpreted as the two ISC populations differing in inherent capacity and fidelity to repair radiation-induced DSB lesions (3, 30–33). Surprisingly, however, we find differences in radiosensitivity result in large part, if not exclusively, from disparities in kinetics of checkpoint recovery. In this regard, small intestinal CBCs begin to exit growth arrest at 12 hours post 19 Gy, and by 15 hours CBCs are dividing at a rate equivalent to that prior to irradiation. Previous studies by Chwalinski and Potten (34), demonstrated synchronous checkpoint recovery of murine small intestinal crypt epithelium with mitotic re-entry *in vivo* after a delay of ~1 hour per Gy, confirmed in our present and previous (13) studies. Here we show this checkpoint recovery kinetic associates with the majority of CBCs initiating cell cycling while still manifesting unrepaired DNA DSBs, as judged by residual γH2AX foci (Fig. 5B shows 60% unrepaired at 12 hours), indicating the Lgr5+ CBC population is subject to the aberrant DDR of checkpoint adaptation. In contrast, the colonic CESC exhibits DDR-regulated checkpoint recovery only at 48 hours post 19 Gy (~2 hour growth delay per Gy), coordinated with completion of DSB repair, as evidenced by resolution of γH2AX foci returning to background levels by 18 hours post radiation. The net outcome of the disparate modes of checkpoint recovery is total depletion of the CBC population by 48 hours and small intestinal organ lethality resulting from denudation of the mucosa, while a significant surviving fraction of CESCs regenerate colonic mucosa and rescue organ function, providing a mechanistic basis for the observed colonic radioresistance relative to the small intestines. The discovery that small intestinal CBCs succumb to checkpoint adaptation is the first demonstration that this aberrant cell cycle response may drive mammalian tissue radiosensitivity.

A number of recent publications in the stem cell literature have attempted to profile radiosensitivity of ISC populations and their cognate intestinal mucosa (30, 31). However, the criteria for defining organ radiosensitivity and the correlation of ISC lethality to organ damage in these studies did not appear to comply with the rigorous criteria, developed and validated over the past four decades by the radiation community, that are used to define inherent radiosensitivity of normal and tumor tissues (3, 32, 33, 35). Hence, while a recent study argues that Lgr5+ stem cells of the colon are more radiosensitive than KRT19+ stem cells of the colon based on differences in post-12 Gy lineage tracing (35), we show that at this dose level colonic Lgr5+ cells are totally resistant to radiation-induced mitotic lethality

and crypt ablation, and hence there is no stress-induced incentive for lineage tracing. We thus posit that the reason lineage tracing is observed in KRT19+ cells is that KRT19 cells undergo significant damage at 12 Gy, leading to KRT19 lineage tracing during the rapid division phase of population recovery. Another less likely possibility is that radiation differentially affects the lineage tracing assay in the KRT19+ and Lgr5+ compartments. Whether or not murine KRT19+ and Lgr5+ stem cells manifest different radiosensitivities or tumors derived thereof will require performance of classic radiation dose survival assays.

In summary, our data broaden and refine the phenotypic features of the Wnt-driven Lgr5+ stem cell populations in the small and large intestine, leading to the discovery that Lgr5+ ISCs in adult murine small intestine are radiosensitive owing to engagement of checkpoint adaptation. These studies thus show that despite a high degree of similarity in vivo and in vitro between the Lgr5+ CBC and CESC, there is nonetheless a major difference in their in vivo response to genotoxic stress, indicating radiation phenotype is organotypic rather than generic for genetic drivers, at least in the context of the Lgr5-Wnt program.

Acknowledgments

Financial support: This work was supported by funds from Mr. William H. Goodwin and Mrs. Alice Goodwin and the Commonwealth Foundation for Cancer Research and The Experimental Therapeutics Center of MSKCC (R.K.), a grant from National Natural Science Foundation of China (31470826) and a gift from the Virginia and D.K. Ludwig Fund for Cancer Research (Z.F.).

References

1. Hill RP, Milas L. The proportion of stem cells in murine tumors. Int J Radiat Oncol Biol Phys. 1989; 16:513–8. [PubMed: 2921157]
2. Kummermehr JC. Tumour stem cells--the evidence and the ambiguity. Acta Oncol. 2001; 40:981–8. [PubMed: 11845964]
3. Baumann M, Krause M, Hill R. Exploring the role of cancer stem cells in radioresistance. Nat Rev Cancer. 2008; 8:545–54. [PubMed: 18511937]
4. Cai WB, Roberts SA, Bowley E, Hendry JH, Potten CS. Differential survival of murine small and large intestinal crypts following ionizing radiation. Int J Radiat Biol. 1997; 71:145–55. [PubMed: 9120350]
5. Wilson JW, Pritchard DM, Hickman JA, Potten CS. Radiation-induced p53 and p21WAF-1/CIP1 expression in the murine intestinal epithelium: apoptosis and cell cycle arrest. Am J Pathol. 1998; 153:899–909. [PubMed: 9736038]
6. Barker N, van Es JH, Kuipers J, Kujala P, van den Born M, Cozijnsen M, et al. Identification of stem cells in small intestine and colon by marker gene Lgr5. Nature. 2007; 449:1003–7. [PubMed: 17934449]
7. Sato T, Vries RG, Snippert HJ, van de Wetering M, Barker N, Stange DE, et al. Single Lgr5 stem cells build crypt-villus structures in vitro without a mesenchymal niche. Nature. 2009; 459:262–5. [PubMed: 19329995]
8. Withers HR, Elkind MM. Microcolony survival assay for cells of mouse intestinal mucosa exposed to radiation. Int J Radiat Biol Relat Stud Phys Chem Med. 1970; 17:261–7. [PubMed: 4912514]
9. Sato T, van Es JH, Snippert HJ, Stange DE, Vries RG, van den Born M, et al. Paneth cells constitute the niche for Lgr5 stem cells in intestinal crypts. Nature. 2011; 469:415–8. [PubMed: 21113151]
10. Potten CS. Radiation, the ideal cytotoxic agent for studying the cell biology of tissues such as the small intestine. Radiat Res. 2004; 161:123–36. [PubMed: 14731078]
11. Hendry JH, Roberts SA, Potten CS. The clonogen content of murine intestinal crypts: dependence on radiation dose used in its determination. Radiat Res. 1992; 132:115–9. [PubMed: 1410267]

12. Qiu W, Carson-Walter EB, Liu H, Epperly M, Greenberger JS, Zambetti GP, et al. PUMA regulates intestinal progenitor cell radiosensitivity and gastrointestinal syndrome. Cell Stem Cell. 2008; 2:576–83. [PubMed: 18522850]
13. Hua G, Thin TH, Feldman R, Haimovitz-Friedman A, Clevers H, Fuks Z, et al. Crypt base columnar stem cells in small intestines of mice are radioresistant. Gastroenterology. 2012; 143:1266–76. [PubMed: 22841781]
14. Lund PK. Fixing the breaks in intestinal stem cells after radiation: a matter of DNA damage and death or DNA repair and regeneration. Gastroenterology. 2012; 143:1144–7. [PubMed: 23000480]
15. Jackson SP, Bartek J. The DNA-damage response in human biology and disease. Nature. 2009; 461:1071–8. [PubMed: 19847258]
16. Bartek J, Lukas J. DNA damage checkpoints: from initiation to recovery or adaptation. Curr Opin Cell Biol. 2007; 19:238–45. [PubMed: 17303408]
17. Shaltiel IA, Krenning L, Bruinsma W, Medema RH. The same, only different - DNA damage checkpoints and their reversal throughout the cell cycle. J Cell Sci. 2015; 128:607–20. [PubMed: 25609713]
18. Dillon MT, Good JS, Harrington KJ. Selective targeting of the G2/M cell cycle checkpoint to improve the therapeutic index of radiotherapy. Clin Oncol (R Coll Radiol). 2014; 26:257–65. [PubMed: 24581946]
19. Durante M, Bedford JS, Chen DJ, Conrad S, Cornforth MN, Natarajan AT, et al. From DNA damage to chromosome aberrations: joining the break. Mutat Res. 2013; 756:5–13. [PubMed: 23707699]
20. Bedford JS, Mitchell JB, Griggs HG, Bender MA. Radiation-induced cellular reproductive death and chromosome aberrations. Radiat Res. 1978; 76:573–86. [PubMed: 569881]
21. Rotolo JA, Maj JG, Feldman R, Ren D, Haimovitz-Friedman A, Cordon-Cardo C, et al. Bax and Bak do not exhibit functional redundancy in mediating radiation-induced endothelial apoptosis in the intestinal mucosa. Int J Radiat Oncol Biol Phys. 2008; 70:804–15. [PubMed: 18191336]
22. Schepers AG, Vries R, van den Born M, van de Wetering M, Clevers H. Lgr5 intestinal stem cells have high telomerase activity and randomly segregate their chromosomes. The EMBO Journal. 2011; 30:1104–9. [PubMed: 21297579]
23. Leibowitz BJ, Qiu W, Liu H, Cheng T, Zhang L, Yu J. Uncoupling p53 functions in radiation-induced intestinal damage via PUMA and p21. Mol Cancer Res. 2011; 9:616–25. [PubMed: 21450905]
24. Kirsch DG, Santiago PM, di Tomasso E, Sullivan JM, Hou W-S, Dayton T, et al. p53 controls radiation-induced gastrointestinal syndrome in mice independent of apoptosis. Science. 2009; 327:593–6. [PubMed: 20019247]
25. Hamilton E. Differences in survival of mouse colon crypts after whole- or partial-body irradiation. Int J Radiat Biol Relat Stud Phys Chem Med. 1977; 31:341–7. [PubMed: 301124]
26. Followill DS, Kester D, Travis EL. Histological changes in mouse colon after single- and split-dose irradiation. Radiat Res. 1993; 136:280–8. [PubMed: 8248486]
27. Benedict SH, Yenice KM, Followill D, Galvin JM, Hinson W, Kavanagh B, et al. Stereotactic body radiation therapy: the report of AAPM Task Group 101. Med Phys. 2010; 37:4078–101. [PubMed: 20879569]
28. Moolenbeek C, Ruitenberg EJ. The "Swiss roll": a simple technique for histological studies of the rodent intestine. Lab Anim. 1981; 15:57–9. [PubMed: 7022018]
29. Castedo M, Perfettini JL, Roumier T, Andreau K, Medema R, Kroemer G. Cell death by mitotic catastrophe: a molecular definition. Oncogene. 2004; 23:2825–37. [PubMed: 15077146]
30. Withers HR. Radiation biology and treatment options in radiation oncology. Cancer Res. 1999; 59:1676s–84s. [PubMed: 10197580]
31. Moore JV, Hendry JH, Hunter RD. Dose-incidence curves for tumour control and normal tissue injury, in relation to the response of clonogenic cells. Radiother Oncol. 1983; 1:143–57. [PubMed: 6680219]
32. Peters LJ. The ESTRO Regaud lecture. Inherent radiosensitivity of tumor and normal tissue cells as a predictor of human tumor response. Radiother Oncol. 1990; 17:177–90. [PubMed: 2181561]

33. Pajonk F, Vlashi E, McBride WH. Radiation resistance of cancer stem cells: the 4 R's of radiobiology revisited. Stem Cells. 2010; 28:639–48. [PubMed: 20135685]

34. Chwalinski S, Potten CS. Radiation-induced mitotic delay: duration, dose and cell position dependence in the crypts of the small intestine in the mouse. Int J Radiat Biol Relat Stud Phys Chem Med. 1986; 49:809–19. [PubMed: 3486164]

35. Asfaha S, Hayakawa Y, Muley A, Stokes S, Graham TA, Ericksen RE, et al. Krt19(+)/Lgr5(−) Cells Are Radioresistant Cancer-Initiating Stem Cells in the Colon and Intestine. Cell Stem Cell. 2015; 16:627–38. [PubMed: 26046762]

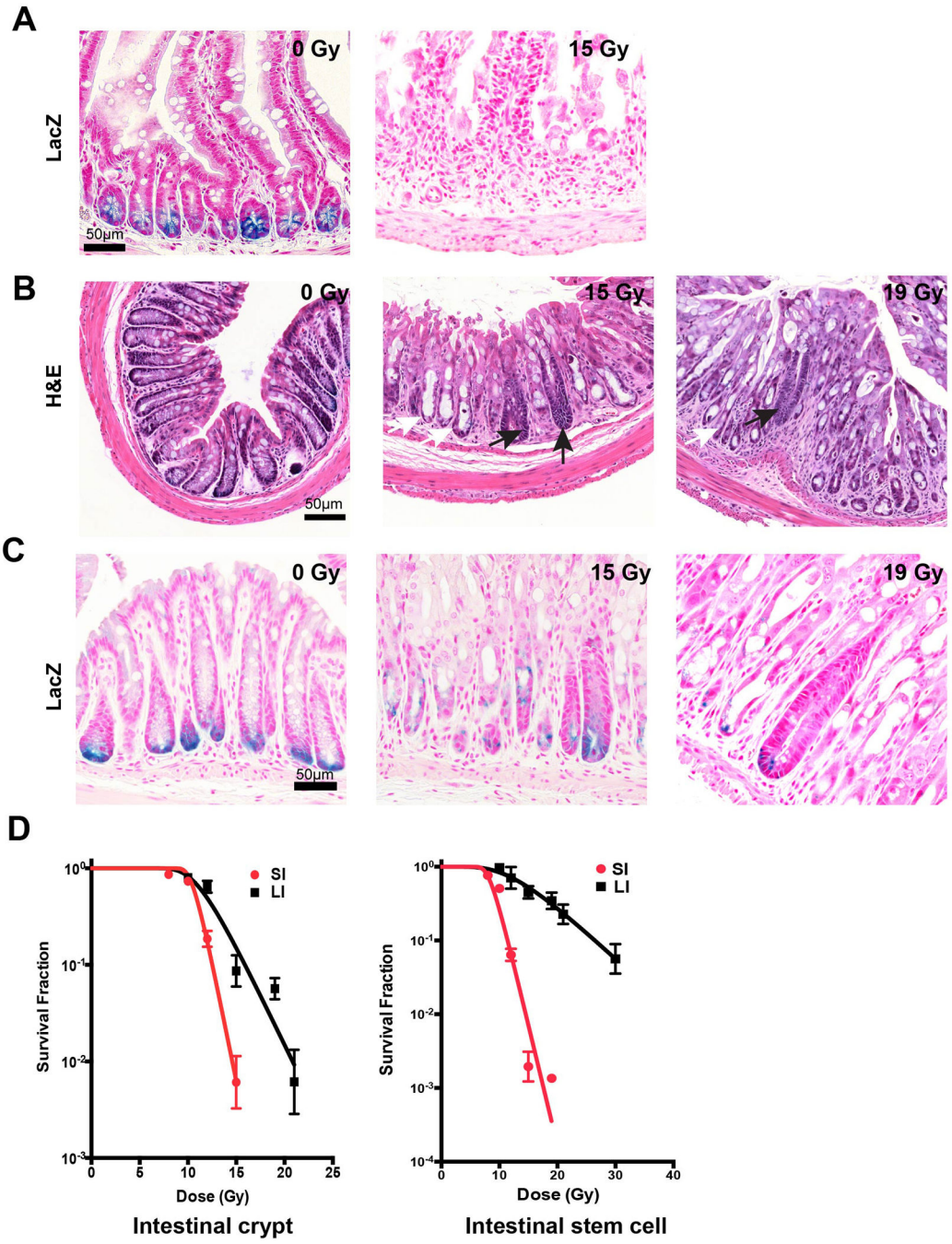

Figure 1. Lgr5+ CESCs in the distal part of large intestine are significantly more radiation resistant than their counterpart in small intestine

(A) LacZ staining of small intestine sections from control and irradiated *Lgr5-lacZ* mice at day 3.5. (B, C) H&E (B) and LacZ (C) staining of distal colon sections from control and irradiated *Lgr5-lacZ* mice at day 5. In B, white arrows indicate degenerating crypts and black arrows indicate regenerating crypts. (D) Quantification of surviving crypts (left) and *Lgr5*+ stem cells (right) in small intestine and distal colon sections from control and irradiated *Lgr5-lacZ* mice at day 3.5 (small intestine) or day 5 (distal colon). Data (mean ±

standard deviation) were quantified from 4 mice/dose, with 3 circumferences/mouse. All panels are of the same magnification; scale bar = 50 μm.

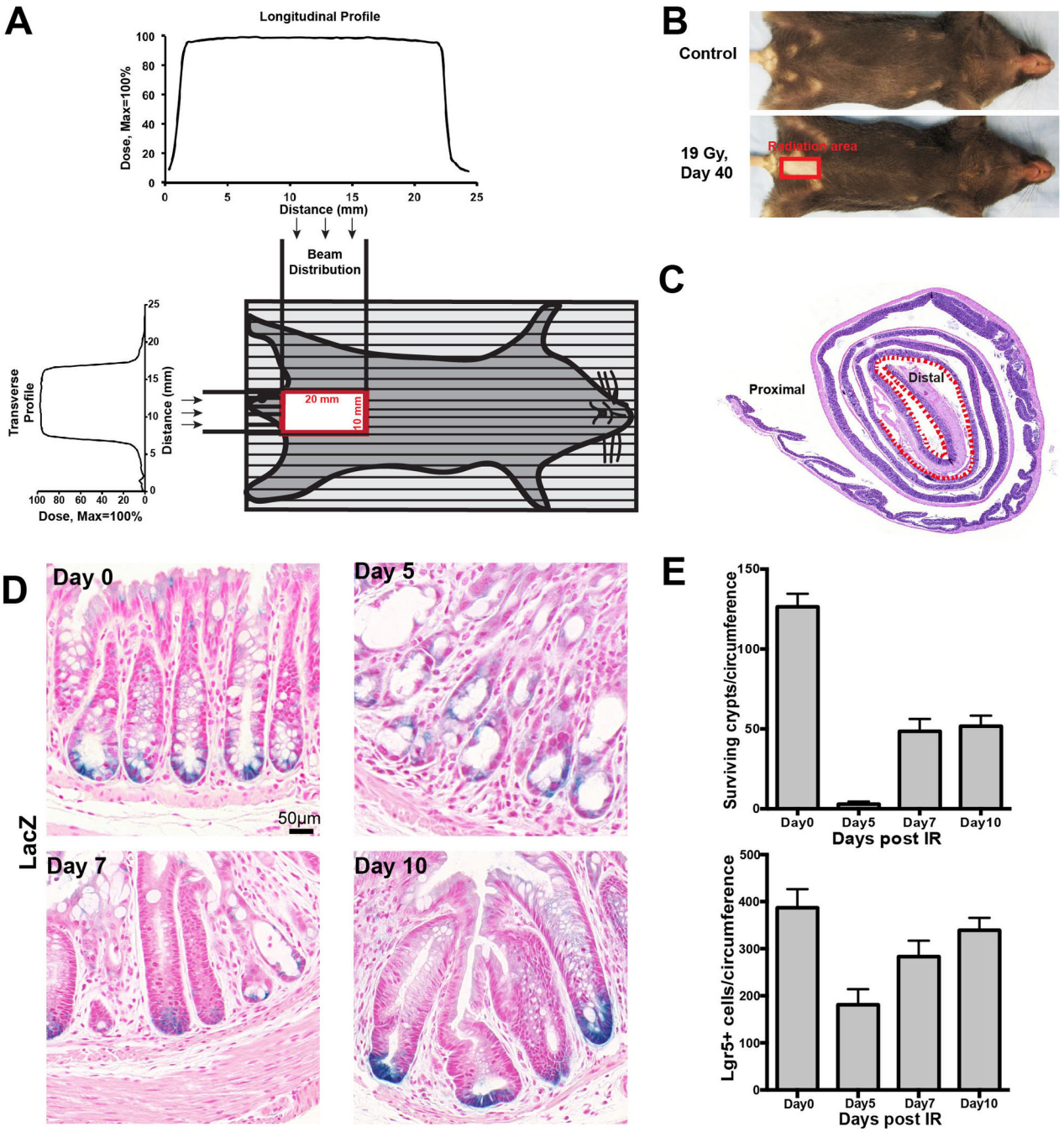

Figure 2. Surviving crypt and *Lgr5*+ CESC kinetic profile after 19 Gy distal colon irradiation

(A) Technique of distal colon irradiation. Schematic presentation of a mouse positioned for irradiation, and the plots of dose uniformity anteroposterior and lateral across the irradiated volume as described in Methods. (B, C) Mice were treated with 19 Gy targeted to the distal colon. In (B), fur loss at 40 days delineates the site of the incident beam at the skin level with sharp margin. In (C), radiation damage to the distal colon mucosa is confirmed by histology at day 5 after 19 Gy (described in Figure 1B) as restricted to the dotted region within the standardized Swiss Roll. (D) LacZ staining of distal colons of *Lgr5-lacZ* mice

treated with 19 Gy distal colon irradiation at day 0, 5, 7 and 10. All images are of the same magnification; scale bar = 50 μm. (E) Quantification of surviving crypts (upper) and *Lgr5*+ stem cells (lower) in distal colon sections of *Lgr5-lacZ* mice irradiated with 19 Gy at day 0, 5, 7 and 10. Data (mean ± standard deviation) were quantified from 4 mice/time point using 3–5 circumferences/mouse.

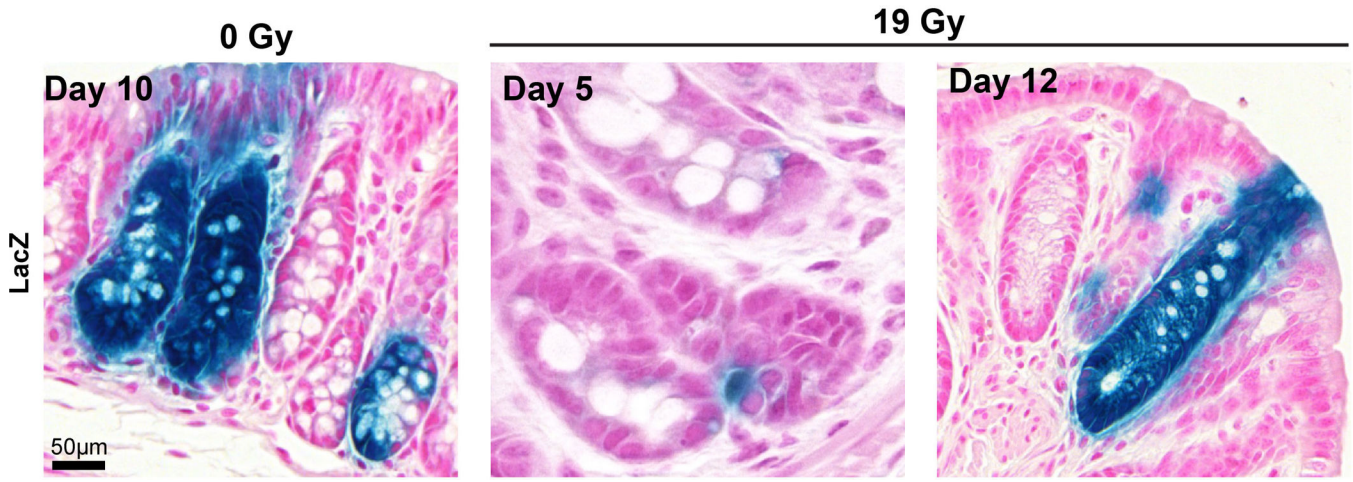

Figure 3. Crypt repopulation originates from Lgr5+ CESCs that survive irradiation

Lineage tracing in distal colon of irradiated *Lgr5-EGFP-ires-CreERT2/Rosa26-lacZ* mice at days 5 and 12 after 19 Gy, or day 10 without irradiation. Adult mice were injected intraperitoneally with a single tamoxifen dose immediately after radiation. All images are of the same magnification; scale bar = 50 μm.

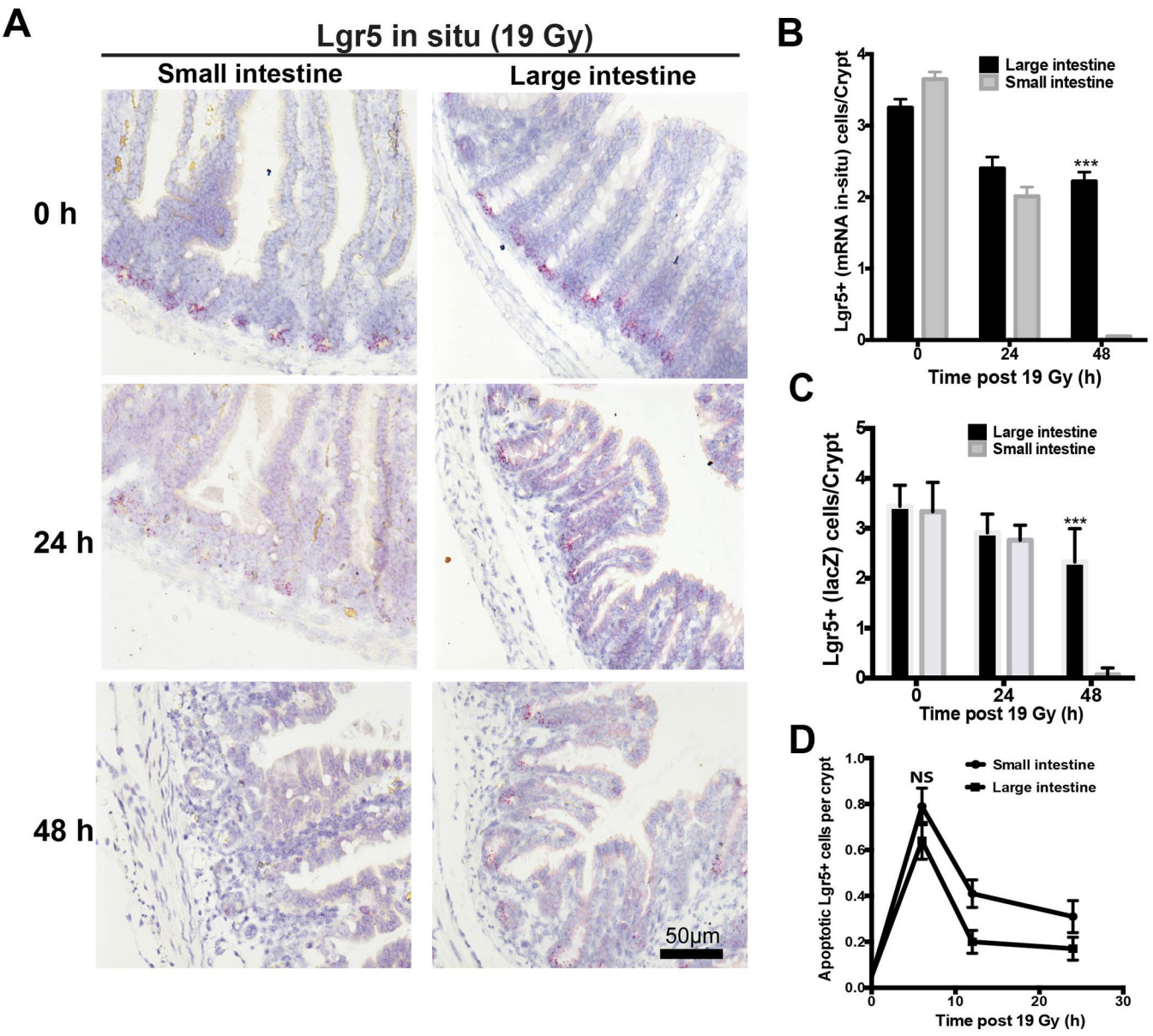

Figure 4. Kinetic analysis of ISC loss

(A) Representative *Lgr5* ISH staining of intestines from *Lgr5-lacZ* mice treated with 19 Gy at day 0, 1 and 2. All images are of the same magnification; scale bar = 50 μm. (B) Quantitative comparison of Lgr5+ ISC depletion, detected by ISH, in the intestines of *Lgr5-lacZ* transgenic mice after 19 Gy irradiation. Bars represent mean ± standard error (n=100 crypts from 4 mice). ***p<0.001. (C) Loss of *Lgr5*+ ISCs was confirmed by *LacZ* staining. Numbers of Lgr5+ positive cells per crypt were quantified from 6 mice/time point, evaluating 50 crypts/mouse. ***p<0.001. (D) Evaluation of apoptotic cell death in ISCs using Lgr5 ISH and caspase3 double staining after 19 Gy irradiation. Bars represent mean ± standard error (n=100 crypts from 4 mice). NS, not significant.

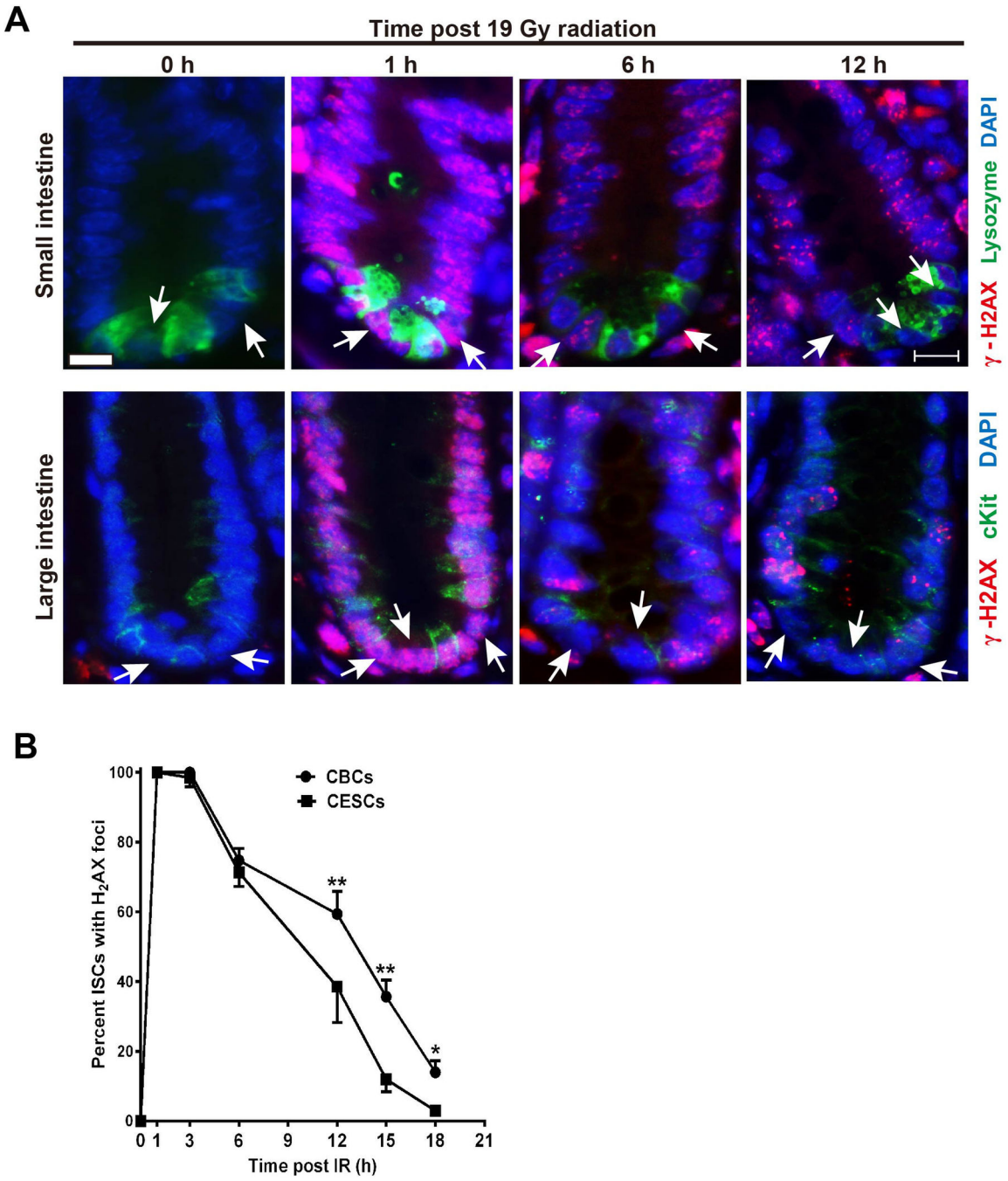

Figure 5. CESCs repair DNA damage more efficiently than CBCs

(A) Representative images of γ-H2AX immunofluorescence staining of intestinal sections in control and irradiated mice at 1h, 6h, and 12h after 19 Gy. Scale bar-10 μm. White arrow indicate ISCs. (B) Quantitative analysis of γ-H2AX focus resolution in CBCs and CESCs cells after 19 Gy WBR. Percent ISCs with γ-H2AX foci was determined by counting CBCs located between lysozyme positive Paneth cells and CESCs located between cKit+ positive Paneth-like cells. Data (mean ± standard error) are collated from 3 experiments analyzing 50 ISCs/mouse and two mice/experiment. **p<0.01, *p<0.05.

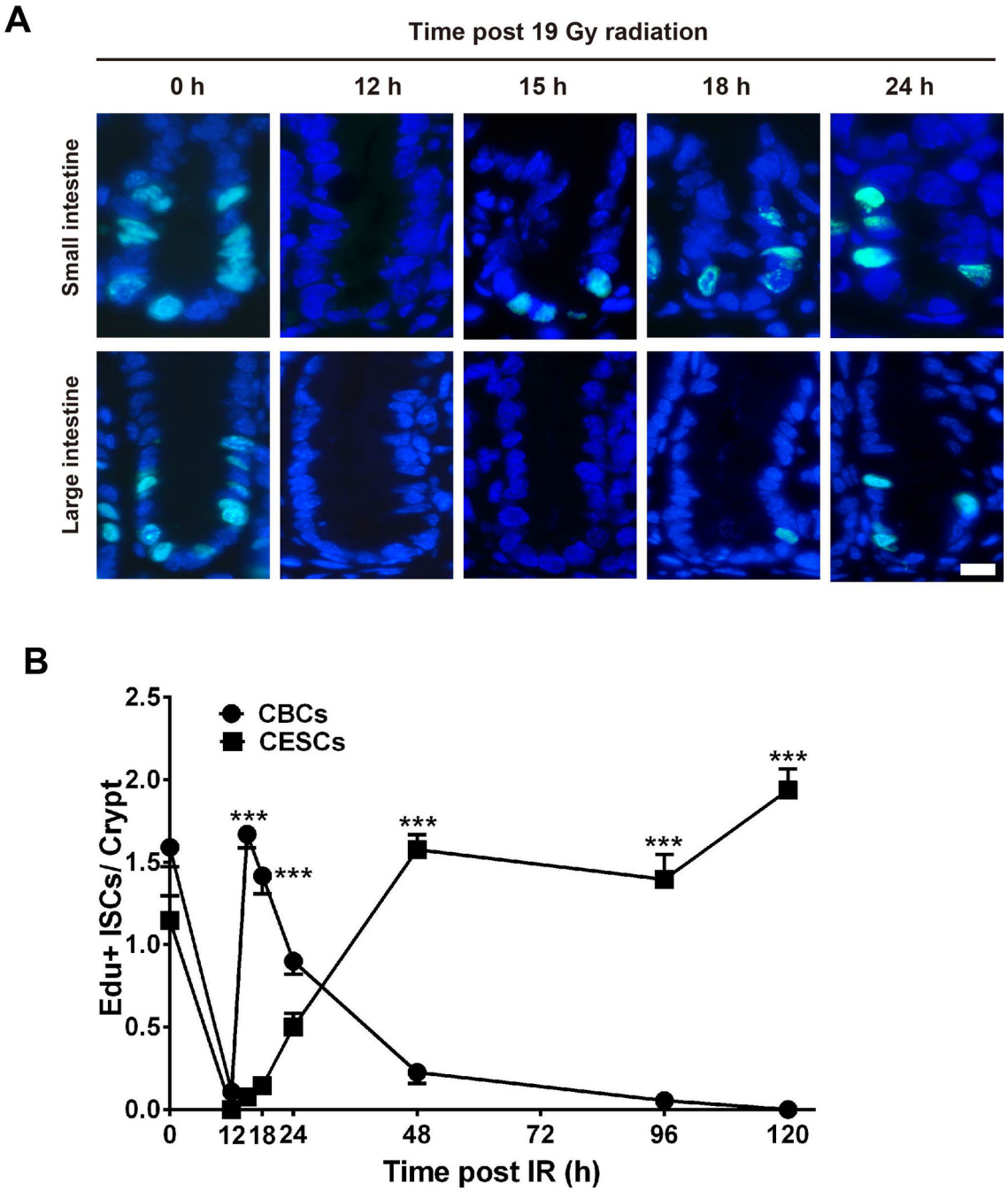

Figure 6. CBCs prematurely exit cell cycle arrest after 19 Gy WBR

(A) Kinetics of ISC proliferation after 19 Gy detected in representative intestinal sections of 8-wk old *Lgr5-lacZ* mice pulsed at the indicated times post irradiation with Edu for 2h before sacrifice. Scale bar-10 μm; (B) Frequency of EdU positive ISCs/crypt in the intestines of *Lgr5-lacZ* mice after 19 Gy. Data (mean ± standard error) are collated from 3 experiments analyzing 100 crypts/mouse using 3 mice/group. ***p<0.001.

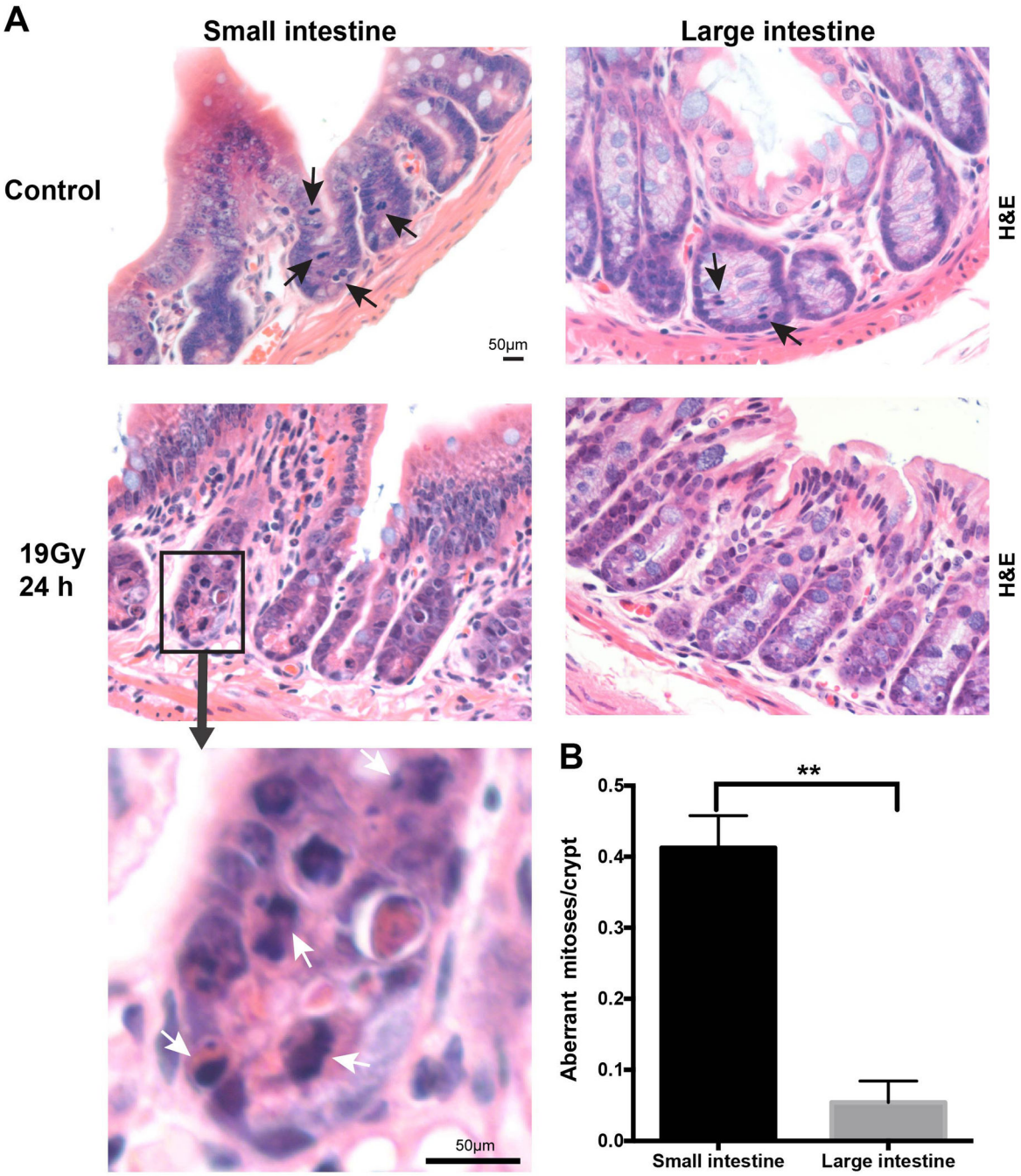

Figure 7. Small intestine crypt epithelial cells display more aberrant mitoses after irradiation compared with large intestine

(A) H&E stained sections of the small intestine and large intestine from *Lgr5-lacZ* mice show normal mitoses in the absence of irradiation and aberrant mitoses 24 hours after 19 Gy WBR. Black arrows indicate normal mitoses and white arrows indicate aberrant mitoses. Upper four images are of the same magnification; scale bar = 50 μm. The insert has a higher magnification, scale bar = 50 μm. (B) Quantification of aberrant mitoses in GI crypt epithelial cells of the small or large intestine. Normal mitoses were scored when a cell was undergoing mitosis and the condensed chromosomes aligned symmetrically. Aberrant

mitoses were scored when condensed chromosomes showed multipolar spindles, lagging or misaligned chromosomes, anaphase bridges, or micronuclei. Mean number of aberrant mitoses per crypt were quantified in a total of 598 small intestine and 810 large intestine crypts from 5 mice. Bars represent mean ± standard error. **$p<0.01$.